The Journal of Experimental Biology 213, 3427-3440

doi:10.1242/jeb.043257

Wake structure and wing kinematics: the flight of the lesser dog-faced fruit bat, *Cynopterus brachyotis*

Tatjana Y. Hubel[1,*,†], Daniel K. Riskin[2,‡], Sharon M. Swartz[1,2] and Kenneth S. Breuer[1]

[1]Division of Engineering, Brown University, Providence RI 02912, USA and [2]Department of Ecology and Evolutionary Biology, Brown University, Providence, RI 02912, USA

*Author for correspondence (thubel@rvc.ac.uk)

[†]Present address: Structure and Motion Laboratory, Royal Veterinary College, Hatfield AL9 7TA, UK

[‡]Present address: Department of Biology, City College of the City University of New York, New York, NY 10031, USA

Accepted 21 July 2010

SUMMARY

We investigated the detailed kinematics and wake structure of lesser dog-faced fruit bats (*Cynopterus brachyotis*) flying in a wind tunnel. High speed recordings of the kinematics were conducted to obtain three-dimensional reconstructions of wing movements. Simultaneously, the flow structure in the spanwise plane perpendicular to the flow stream was visualized using time-resolved particle image velocimetry. The flight of four individuals was investigated to reveal patterns in kinematics and wake structure typical for lower and higher speeds. The wake structure identified as typical for both speed categories was a closed-loop ring vortex consisting of the tip vortex and the limited appearance of a counter-rotating vortex near the body, as well as a small distally located vortex system at the end of the upstroke that generated negative lift. We also investigated the degree of consistency within trials and looked at individual variation in flight parameters, and found distinct differences between individuals as well as within individuals.

Supplementary material available online at http://jeb.biologists.org/cgi/content/full/213/20/3427/DC1

Key words: bat flight, kinematics, wake structure.

INTRODUCTION

Considerable effort has been expended to gain understanding of force generation by flapping wings. Although investigations of manufactured wings and mechanical models inspired by insects and birds (van den Berg and Ellington, 1997; Dickinson et al., 1999; Hubel and Tropea, 2009) provide basic insight into flow conditions and the development of aerodynamic forces over moving wings, only studies of living animals can reveal the actual kinematics and aerodynamics of insect, bird and bat flight. Direct force measurements are commonly used to shed light on instantaneous net forces generated on model wings, but, with the exception of certain insects, this approach is not realistic for animal flight because the measuring apparatus requires that the flying animal be tethered in a manner that will intrinsically alter flight performance for most flying animals.

Fortunately, improvement in modern laser measurement techniques provides the opportunity for non-invasive force estimates based on optical measurement of the flow field behind an animal flying in a very natural fashion. Particle image velocimetry (PIV) has been used to study the flow around and behind insect and bird wings in detail (Spedding et al., 2003a; Spedding et al., 2003b; Warrick et al., 2005; Hedenström et al., 2006; Henningsson et al., 2008; Johansson and Hedenström, 2009) and has provided insight into the force generation and the importance of unsteady effects such as additional lift generation due to leading edge vortices (Birch and Dickinson, 2001; Birch and Dickinson, 2003; Bomphrey et al., 2005; Lu et al., 2006). In addition to PIV, high speed videography has also been used to reveal the detailed motion of the wings, providing insight into the motion itself, as well as, in some cases, elastic deformations due to aerodynamic and internal forces. These approaches and others have been applied with great success to insect and bird flight in the engineering and biological communities over the last two decades (Dickinson and Gotz, 1996; Ellington, 1999; Usherwood and Ellington, 2002; Sane, 2003; Spedding et al., 2003a; Tobalske et al., 2003; Usherwood et al., 2003; Tobalske et al., 2007).

By contrast, the investigation of bat flight is still in its early stages. Several kinematic studies on bats have been carried out (Norberg, 1976a; Norberg, 1976b; Aldridge, 1986; Lindhe Norberg and Winter, 2006; Iriarte-Diaz and Swartz, 2008; Riskin et al., 2008; Riskin et al., 2009; Wolf et al., 2010) providing the basis for the prediction of aerodynamic forces, however, few studies include the actual measurement of the wake structure. So far, only three species have been investigated more closely with regards to their wake structure: two relatively small nectar-feeding, phyllostomid, echolocating bats, *Glossophaga soricina* (10 g) and *Leptonycteris* sp. (20 g) (Hedenström et al., 2007; Johansson et al., 2008; Muijres et al., 2008; Hedenström et al., 2009), and *Cynopterus brachyotis*, a medium sized (30–40 g) non-echolocating pteropodid fruit bat (Tian et al., 2006). Consequently, relatively little is known about the wake structures typical of bat flight, and even less about the correlations between wing kinematics and wake structure. Variation between individuals of the same species has gained very little attention so far. Limitations in measurement technology, such as low PIV recording frequencies and hence time-consuming measurements have resulted in a very low sample sizes, often as few as two individuals. While these are a valuable starting point and have provided considerable knowledge about the importance of certain flight parameters and the nature of vortex patterns, there is a need to investigate several individuals to gain an understanding about possible variations and tolerances in kinematics and force generation within a single species. High-speed PIV recordings not only make it possible to increase the number of individuals

investigated because of faster data collection, they also make it possible to follow the time-resolved development of single wingbeat cycles, avoiding errors and uncertainties due to the reconstruction of a wingbeat cycle from several distinct realizations (Hedenström et al., 2009; Hubel et al., 2009). In addition, they alleviate the problem of investigating animals that cannot easily be trained to fly at a fixed position, such as non-hovering bat species.

Here, we report on a study in which we have measured the wake structure in the spanwise (or transverse) plane behind four *Cynopterus brachyotis* in two different flight speed ranges. Using time-resolved PIV with a sampling rate of 200 Hz, we were able to capture approximately 30 PIV images over each wingbeat cycle. Synchronized with the PIV data, three-dimensional (3-D) wing motion was then reconstructed to provide information about kinematic parameters such as flapping frequency, angle of attack, amplitude etc., in addition to the precise spatial location of vortex structures and anatomical landmarks of the wing. The current study greatly extends the initial demonstration of time-resolved PIV by our group (Hubel et al., 2009), providing significantly more detail on the wake vortex structure and kinematics, as well as considerable detail regarding variation between individuals in both kinematics and wake patterns.

MATERIALS AND METHODS

Bats

Four captive-bred female lesser dog-faced fruit bats, *Cynopterus brachyotis* (Müller 1838), were trained to fly in the low-speed wind tunnel in the Division of Engineering at Brown University, RI, USA. Each bat was flown at least twice a week over the period of the study. All experiments were conducted with the authorization of the Institutional Animal Care and Use Committees of Brown University, the Lubee Bat Conservancy, and the Division of Biomedical Research and Regulatory Compliance of the Office of the Surgeon General of the United States Air Force.

The body mass of each bat was measured before the recording session. Both the morphological characteristics of each bat and the wingbeat cycle descriptors were determined directly from in-flight kinematic measurements (described below). Wing span was defined as twice the maximum distance between body midpoint (see below for definition of anatomical landmarks) and the wingtip, and the wing chord was defined by the maximum distance between wrist and tip of the fifth digit. We calculate the chord in this way because wing extension changes greatly over the course of the wingbeat cycle, in contrast to a much smaller change in this anatomically defined wing chord. A calculation of wing chord based on extension and area would therefore be misleading, especially considering the uncertainty in the area calculation resulting from wing curling. The anatomical chord is, in this case, a considerably more reliable value. However, for comparison, we also provide the chord value based on wing area and wingspan averaged over the wing beat cycle. A mean and standard deviation were calculated for chord, span and mass of all bats (Table 1). Span and chord were calculated using the first wingbeat cycle when the bat was in the field of view of both kinematic and PIV cameras.

Table 1. Mean and standard deviation of span, chord and mass of the four study subjects

	Span b (m)	Chord c (m)	Chord $c_{Aw/b}$ (m)	Mass m (g)
Bat I	0.171±0.003	0.075±0.001	0.057±0.003	30.0±1.0
Bat II	0.171±0.004	0.078±0.001	0.063±0.003	31.3±2.1
Bat III	0.180±0.006	0.084±0.001	0.058±0.01	38.3±1.3
Bat IV	0.172±0.004	0.084±0.001	0.053±0.005	36.3±0.1

Wind tunnel

The measurements were conducted in a closed-circuit wind tunnel with the test section having a cross section of 0.60 m×0.82 m (height × width) and a length of 3.8 m. The original low free-stream turbulence level of 0.08% was increased to 0.5% by the installation of a fine-mesh (600 wires per meter) net at the upstream entrance to the test section to prevent the bats from entering the settling chamber (Hubel et al., 2009). The mesh generates an array of jets ($Re \sim 400$ at 5 m s^{-1}) which quickly merge to form a very fine-grained turbulent background noise and, although this turbulence level was somewhat greater than that of the net-free flow, the mesh did not generate structured, coherent wakes, as has been seen in some instances (i.e. Spedding et al., 2009), and did not affect the bat flight in any discernable manner. The bats were introduced into the section by hand at the downstream end of the test section. They flew upstream and landed on a screen mesh that was offered to them after they passed through the measurement volume. Experiments were conducted at two wind speeds: 3.8 and 5.8 m s^{-1}. After accounting for the additional speed of the bats, the resulting average flight speeds were 5.0±0.1 m s^{-1} and 6.7±0.4 m s^{-1} (mean ± s.d.).

The limited observation area required the bat to fly close to the geometric center of the cross section of the test section to be able to successfully record PIV images of one or more wingbeat cycles. No corrective maneuvers were necessary or observed for these consecutive wingbeat cycles. Ground effects have been reported to be significant for a dimensionless height, $\beta_G<0.5$ [β_G=height (h)/wing semispan (b)] while having very little effect for $\beta_G>1$ (Rayner, 1991). Flying in the middle of the test section, β_G was calculated to be above 1.5 for our bats, therefore any ground and wall effects have been assumed to be negligible.

A right-handed coordinate system was defined in which positive x was defined in the direction of the wind (negative in the flight direction of the bat). The y-coordinate is positive from center of the bat towards the tip of the right wing, and the z-coordinate is positive in the vertical upward direction.

Depending on the particular analysis, results are presented in (1) a bat-centered coordinate system with the origin located at the body marker centered between the scapulae, roughly 1.5 cm caudal to the skull, (2) a wind tunnel-fixed coordinate system, or (3) a combination coordinate system, in which the y- and z-coordinates are in the bat-centered system but the origin of the x-axis is fixed at the plane where PIV measurements were acquired.

Kinematics

The movements of the bats' bodies and wings were recorded using three Photron 1024 PCI high speed cameras (1024×1024 pixels, 200 f.p.s., shutter speed 1/1000 s; Photron USA, Inc., San Diego, CA, USA), synchronized with the PIV recordings. Two halogen lamps were used for illumination, pointing away from the PIV cameras so as to minimize light pollution. Red filters were placed over the lights so that light for high-speed video did not interfere with the shorter wavelength light used for PIV, and so that the lights were less disruptive to the bats. The kinematic camera calibration was achieved by calculating the direct linear transformation (DLT) coefficients (Abdel-Aziz and Karara, 1971) by manually tracking 144 calibration markers in four different planes within the measurement volume.

Kinematics measurements were obtained by tracking high-contrast markers which were non-toxic white paint on five locations

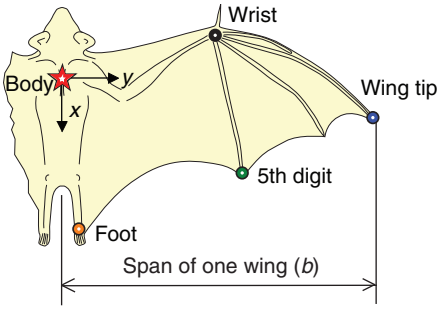

Fig. 1. Marked positions on the dorsal surface of the bat.

on the bat: the midline of bat's body, overlying the vertebral column and midway between the scapulae; the right foot at the ankle joint; the right carpus; the tip of the distal phalanx of right digit III; and the tip of the distal phalanx of right digit V (Fig. 1).

Each marker was tracked in each camera view to obtain 2-D coordinates; gaps in the data resulting from obstruction of the markers were then filled using a third-order polynomial. 3-D coordinates were calculated based on the DLT coefficients and validated by projecting them on all three camera views. Complete wingbeat cycles within one trial were identified and subdivided according to the upper reversal point of the wingtip. Each wingbeat cycle contained approximately 28–32 kinematic frames, but because of the Doppler effect 34–37 PIV frames were recorded (see below: Correlation of kinematics and PIV). For ease of analysis, all wingbeat cycles were interpolated in order to achieve a uniform number of 35 frames per cycle.

Based on the motions of the body markers, the velocity and acceleration of the bat were calculated in the global coordinate system. The horizontal speed of the bat, $\mathbf{U}_B$, was calculated as the distance traveled in the *x*-direction during a complete wingbeat cycle, divided by travel time. This value was negative because it refers to travel in the negative, upstream direction in the global coordinate system. The ground speed, $\mathbf{U}_t$, was calculated from the combination of the wind speed ($\mathbf{U}_\infty$) and the bat's true air speed ($\mathbf{U}_B$): $\mathbf{U}_t=\mathbf{U}_\infty-\mathbf{U}_B$. The horizontal and vertical accelerations, $\mathbf{a}_x$ and $\mathbf{a}_z$ respectively, were calculated from the change in horizontal and vertical velocities observed over a full wingbeat cycle.

Additional parameters calculated in the global coordinate system were the wingbeat period, *T*, and its reciprocal, the flapping frequency, *f*, as well as the geometric angle of attack, α_g. The wingbeat period, *T*, was defined as the time between two consecutive upper reversal points of the wingtip. The geometric angle of attack, α_g, was defined as the angle between the resultant flow due to flapping, forward flight and wind tunnel speed and the chord line. The chord line was determined by the wrist position and the corresponding location on the trailing edge parallel to the body, between the foot and the fifth digit.

The global coordinate system was transformed to a body-referenced coordinate system by subtracting the body marker position from the global coordinates, and additional flight parameters were calculated. The downstroke ratio, τ, was defined as downstroke period divided by the total wingbeat period based on the wingtip motion in the *z*-direction. The wing stroke amplitude, θ_{tip}, defines the maximum angle between wingtip positions relative to the midline body marker on the bat's back over the course of a wingbeat cycle. Although many studies of bat flight kinematics define wingbeat amplitude measurements by movements of the wingtip or wrist with respect to the shoulder, markers on the skin at the shoulder are subject to greater skin motion relative to the position of the joint than markers on the body or wing (Riskin et al., 2008). Moreover, the shoulder moves relative to the spine because the clavicle participates significantly in the skeletal motion of the wingbeat, hence the shoulder motion is a meaningful element of the wing motion in bats. We therefore chose the midline body marker as our reference, finding that it gives us a repeatable and intuitive measurement of wing stroke amplitude. Assuming a constant distance between the body marker and the shoulder joint over the wing beat cycle, we estimate amplitude based on the shoulder to be roughly 5.6 deg larger than that based on the body marker.

Stroke plane angle, β, is the angle between the horizontal and a linear regression line fitted to the wingtip trajectory of the wingtip in the *x*–*z* plane. It was also useful to monitor the wing-retraction (how close the bat pulled its wing to its body during the upstroke) and for this, the minimum body-to-tip distance, d_{min}, was defined as the minimum 3-D distance between body marker and wing tip. Finally, the Reynolds number, $R=\mathbf{U}_\infty c/\nu$ and reduced frequency, $k=\pi fc/\mathbf{U}_\infty$, were calculated as well.

Span ratio, *SR*, is the ratio of wing span in up- to downstroke, and was calculated for the wing passing through the horizontal plane. However, the span ratio gives no information about curling, a motion occurring distal to the elbow, as a result of flexion of the metacarpophalangeal and interphalangeal joints, and, perhaps, deformation of the elongated, slender phalanges. In our opinion, curling is better expressed by the minimum distance between wing tip and body, not necessarily occurring at mid-upstroke.

Particle image velocimetry

The PIV measurements were performed using a 200 Hz double-pulse Nd:YAG laser (Litron LPY 703-200/100, 532 nm; Rugby, UK), synchronized with the kinematics cameras. Di-ethyl-hexyl-sebacate (DEHS) was used for particle generation using a custom-built fog generator with a Laskin-type nozzle (particle size ~1 μm). The displacement of the seeding particles was recorded with two high-resolution CMOS cameras (Photron 1024 PCI, resolution 1024×1024 pixels) equipped with band-pass filters. These two PIV cameras were located perpendicular to the flow stream at the end of the test section, and thus observed the wake structure in the *y*–*z*-plane. The two cameras were stacked in the vertical direction, capturing two slightly overlapping images that were merged together afterwards to accommodate the large size of the observation area necessary to capture a whole wingbeat cycle (0.23 m×0.41 m width×height). Stitching of the two images was accomplished by using the stitching tool in the DaVis software.

To reduce any effect of parallax error that may arise from carrying out 2-D PIV in cross-stream flow, we carried out a subtraction of background flow prior to merging the velocity fields from the two cameras. This change in processing resulted in only a 4% change in total circulation. Owing to the large size of the observation area, any parallax displacement was less than one-tenth of a pixel displacement which is near the limits of resolution for this PIV setup and therefore had negligible effect on our measurements. Furthermore, parallax effects have little influence on wake structure interpretations based on the vorticity fields, making this approach an especially suitable solution to the challenge of describing the relatively large wakes generated by bats of this body and wing size.

Limited pulse energy and camera resolution requires a compromise between image quality and size of the observation area, restricting wake capture to the area between body and right wing. The wake structure was mirrored under the assumption that left and right wings generate similar circulation in steady forward flight. This approach will necessarily impose a symmetrical wake structure

even where slight difference between right and left wing would have been present but not recorded, but given that the PIV observation area is limited and that all trials analyzed were straight or nearly straight flight, we believe mirroring the wake is physically appropriate. Mirroring of the smoothed swirl field occurred along the line of the body trajectory at the body marker position, in the x–z-plane.

Because of the risks to the bats from the energy-intense PIV laser, a laser-light safety curtain was installed 0.05 m upstream of the PIV laser-illuminated cross section, gating the operation of the PIV system. The safety light curtain consists of an array of 21 low-power red diode lasers spanning the entire test section, each aimed at a complementary photodiode. Breaking one of the beams resulted in blocking the Q-switch signals, shutting the PIV system down to prevent any potential harm to skin and eyes of the bats.

The PIV space was calibrated using the same calibration plate as was described above for the kinematics system. Using a single calibration plate with the origin of the coordinate system visible in both kinematics and PIV cameras allowed for simultaneous but independent calibrations, greatly simplifying image synchronization. The calibration parameters are achieved by using a pinhole calibration (Hartley and Zissermann, 2000).

The PIV measurement sequence was initiated using a manually operated trigger which was activated once the bat was observed to safely fly upstream of the location of the laser light sheet. The trigger enabling the safety curtain was switched on, which subsequently enabled the PIV laser, which continued to fire as long as the bat flew away from the laser light. Several seconds of PIV and data could be acquired, which was sufficient to allow the bat to fly through the kinematic measurement volume, and to land on the retrieval net approximately 1 m further upstream.

The PIV images were recorded and analyzed using DaVis 7.2 software (LaVision). Vector fields were calculated using sequential cross-correlation with multi-pass iterations with decreasing size (128×128, two iterations to 64×64, two iterations, 50% overlap). Post processing consisted of the replacements of vectors with peak ratio Q<1.2 and average neighborhood variation >1.5×rms using interpolation and the application of a simple 3×3 smoothing filter. Subsequently, the vector fields were exported and processed in Matlab (The Mathworks, Inc., Natick, MA, USA).

The vorticity and swirl (the rotational part of the local two-dimensional rate-of-strain tensor), were calculated in order to visualize the development of wake structure over time. The vorticity was calculated in the following manner:

$$\boldsymbol{\omega}_x = \frac{d\mathbf{v}}{dz} - \frac{d\mathbf{w}}{dy}\ , \tag{1}$$

where $\mathbf{v}$ and $\mathbf{w}$ are the velocity components in the y- and z-directions.

Vorticity contains both rotation and shear information, hence the swirl was used to minimize noise in the isosurface reconstructions by showing only the rotational part of the vortex (Adrian et al., 2000). The swirl was calculated in the following manner:

$$\text{swirl} = \left(\frac{\partial \mathbf{v}}{\partial z}\cdot\frac{\partial \mathbf{w}}{\partial y}\right) - \frac{1}{2}\left(\frac{\partial \mathbf{v}}{\partial y}\cdot\frac{\partial \mathbf{w}}{\partial z}\right) + \frac{1}{4}\left(\left(\frac{\partial \mathbf{v}}{\partial y}\right)^2 + \left(\frac{\partial \mathbf{w}}{\partial z}\right)^2\right). \tag{2}$$

Only the positive part of the swirl was used, while the negative part, representing the shear, was set to zero. In displaying results, isosurfaces of swirl are used to show a 3-D reconstruction of the wake structure based on the 2-D PIV measurements in the y–z-plane. Since swirl is always positive and therefore cannot distinguish between clockwise and counterclockwise rotating vortices, sign was chosen based on the vorticity template. The surfaces were plotted using a 3×3 smoothing filter and swirl threshold (±25) that allowed the vortex structures to be visualized but reduced the remaining noise. The body marker between the scapulae of the bat was chosen as point of origin in y–z-plane and each PIV image was adjusted accordingly; time was converted into streamwise distance by assuming that the wake structures advected with the freestream velocity. The increasing distance due to the additional speed of the bat was determined for each frame and the Doppler effect was taken into account (see below, Correlation of kinematics and PIV).

Circulation, Γ, over different areas of the flow field was calculated by integrating the vorticity, $\boldsymbol{\omega}_x$, over a defined area, A, as:

$$\Gamma = \iint_A \boldsymbol{\omega}_x dA\ . \tag{3}$$

The total circulation was calculated by taking the whole area to the right of the body marker into account. In addition, we have identified four distinct, recurring vortices (see below, Correlation of kinematics and PIV). To separate vortices from background noise and from each other, a threshold of $\pm 5\ \text{s}^{-1}$ was applied to the vorticity field and values below the threshold were set to zero. The threshold value of $\pm 5\ \text{s}^{-1}$ was chosen to maximize separation among the distinct vortex structures and of vortices from background noise, while accounting for as much vorticity as possible. For each of the four reoccurring vortices, location was determined manually in each of the approximately 30 vorticity fields collected for each wingbeat, and in each case, the circulation was calculated based on all contiguous positive or negative vorticity at the chosen location. In the few cases where V1 and V3 could not be separated from each other by using the threshold of $5\ \text{s}^{-1}$, the circulation of V3 was assumed to equal that of V4 and the value was subsequently subtracted from the circulation calculated for the tip vortex. The lift associated with the streamwise vortex was calculated from the instantaneous circulation, Γ_i, based on the instantaneous wing span, $2b_i$, as:

$$\mathbf{Fz}_i = \rho\Gamma_i \mathbf{U}_\infty 2b_i\,, \tag{4}$$

where ρ is the density of the air and b is the span of one wing. Subsequently the force was averaged over the course of the wing beat cycle. One needs to consider that the circulation extracted from the transverse plane contains only the vertical force component of the lift, and that the magnitude of the horizontal force component is not determined. This is a rather simple model for the lift force, ignoring several issues, such as the influence of the near-body vortex and the distal vortex pair, as well as the fact that unsteady fluid effects, such as virtual mass, may play a role in the generation of lift. However, the chief goal of this work is to elucidate wake structure, not to determine the absolute magnitude of the lift force, hence this model is sufficient to provide some correspondence between vortex strength and the nominal lift generated.

Correlation of kinematics and PIV

A key feature of these experiments is the synchronized acquisition of both the flight kinematics and the wake velocity structure. However, the correlation of specific features in the wake with body and wing motions is not trivial and fraught with complexities. To determine the features on the body and the phase of the wingbeat cycle associated with a particular vortex structure in the wake, one needs to know the distance between the bat and the PIV laser sheet and a characteristic velocity at which the vortex structures are advected downstream. The distance is easily determined from the synchronized flight kinematics, and it is usually adequate to use the wind tunnel freestream speed, $\mathbf{U}_\infty$, as the typical advection speed. The distance and speed yield a time offset between the recorded

kinematics and the associated PIV velocity measurement. However, the situation is made more complex by the fact that the bat is not at a fixed distance from the PIV laser sheet, but usually flies upstream. This produces a 'Doppler shift' in the time-resolved PIV fields, which is corrected by determining an effective PIV sample time: $dt_{new}=dt\times\mathbf{U}_\infty/\mathbf{U}_t$ (Hubel et al., 2009). Lastly, when there are intense levels of vorticity, the assumption that vortex structures are advected straight downstream is probably not valid, as the structures will be shifted by the flow induced by adjacent vortices. This induced motion is relatively small for short distances between the bat and the PIV laser measurement position and during the bulk of the downstroke when the wing is outstretched and the primary vortex is far from other vortex structures. However, the possible change in position should be considered, particularly when trying to correlate kinematics with flow structures when the wings are retracted and the vortex structures are in close proximity to each other.

Statistics

Flight trials varied in speed, with a clearly bimodal distribution; each bat flew at both a lower and a higher speed, with some variation around that speed, and some variation among bats. Because the flight speed distribution was clearly bimodal, it was not appropriate to treat speed as a continuous variable. Instead, we tested for differences in kinematic parameters between the two observed speed categories. A single trial could contain up to six wingbeat cycles. To assess differences in means between the two speed categories at a significance level of 5%, we used 60 wingbeat cycles, and employed a mixed effect model with wingbeat cycle as a repeated measure and individual as a random effect to account for pseudoreplication. Means are presented ±s.d. All tests were carried out using SPSS 17.0 (SPSS Inc., Chicago, IL, USA).

Data presented over the course of a wingbeat cycle were calculated based on five wingbeat cycles for each bat in both speed categories (only three for Bat IV at higher speed). We chose only one wingbeat cycle – the first with both PIV and kinematic data available – in order to avoid pseudoreplication within trials. The average over the five wingbeat cycles was calculated within the individual bats, and subsequently mean and standard deviation for all four bats are presented.

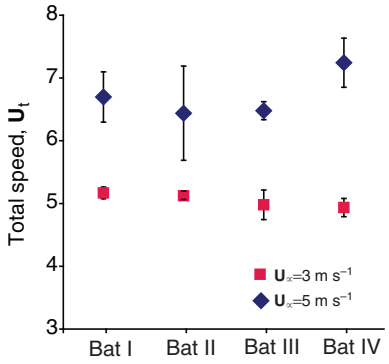

Fig. 2. Resulting total speed, $\mathbf{U}_t$, and standard deviation for four bats.

RESULTS

Kinematics

The effective flight speed, based on the wind speed and the bat motion relative to the test section, showed that all bats flew distinctly faster than the wind tunnel speed. At the lower wind speed (3.8 m s^{-1}) they flew upstream at approximately 1.3 m s^{-1}, whereas at the higher wind speed (5.8 m s^{-1}) they added only an average of 0.8 m s^{-1}, bringing the total flight speeds to 5.0±0.1 m s^{-1} (*Re*~19,000, *k*~0.57) and 6.7±0.4 m s^{-1} (*Re*~25,500, *k*~0.42; Fig. 2). These resulting speeds were distinctly different from each other and represent two discrete flight speeds at the lower end and middle of the range of flight speeds observed for this species. The higher speed was accompanied by a significant increase in wingbeat amplitude, whereas the stroke plane angle, maximal wing extension, minimum body-tip distance and geometric angle of attack at mid-downstroke were all significantly higher in the lower speed category (Table 2). There was no significant change in flapping frequency and downstroke ratio. No significant differences between the two flight speeds were observed in either the vertical or horizontal accelerations and the average acceleration was small, as expected for steady flight. The standard deviations were high because of a small number of trials that showed higher accelerations in both horizontal and vertical directions, with values up to $\mathbf{a}_x$=3 m s^{-2} and $\mathbf{a}_z$=8 m s^{-2}. Trials with higher acceleration were not excluded from the analyses

Table 2. Comparison of kinematic parameters between lower and higher speed flights for all bats

	Lower speed *n*=22		Higher speed *n*=38	d.f. *n*=60	*t n*=60	*P*-value *n*=60
Frequency, *f* (Hz)	8.19±0.29		8.02±0.29	35.3	0.79	0.436
Amplitude, θ_{tip} (deg)	50.6±3.1	<	64.5±3.1	34.0	–5.31	<0.001
Downstroke ratio, τ (–)	0.50±0.01	>	0.48±0.01	34.0	2.21	0.034
Horizontal acceleration, $\mathbf{a}_x$ (m s^{-2})	0.30±0.16		0.37±0.15	34.0	0.33	0.743
Vertical acceleration, $\mathbf{a}_z$ (m s^{-2})	–0.84±0.29		–0.90±0.25	27.9	0.16	0.872
Stroke plane angle, β (deg)	–56.9±3.2	>	–64.3±3.2	32.0	4.82	<0.001
Max. span (one wing), *b* (m)	0.177±0.003	>	0.173±0.003	27.7	3.07	0.005
Max. wing chord, *c* (m)	0.08±0.002		0.08±0.002	36.2	–1.52	0.138
Min. distance body – wing tip, d_{min} (m)	0.09±0.008	>	0.07±0.0087	33.2	5.07	<0.001
Span ratio *SR* (–)	0.60±0.033		0.62±0.021	33.4	–0.12	0.097
Geometric angle of attack, α_g (deg)	22.0±1.6	>	16.6±1.5	32.7	6.92	<0.001
Circulation A_t, Γ (m^2 s^{-1})	0.074±0.007	>	0.050±0.007	30.2	5.36	<0.001
Circulation V1, Γ (m^2 s^{-1})	0.085±0.014	>	0.057±0.014	35.2	3.73	0.001
Circulation V2, Γ (m^2 s^{-1})	0.007±0.004		0.007±0.004	28.9	–0.67	0.509
Circulation V3, Γ (m^2 s^{-1})	0.008±0.002		0.006±0.002	45.4	1.50	0.147
Circulation V4, Γ (m^2 s^{-1})	0.005±0.001		0.004±0.001	42.2	–1.43	0159

Values are means ± s.d.; *n*, number of wingbeat cycles used for calculation.

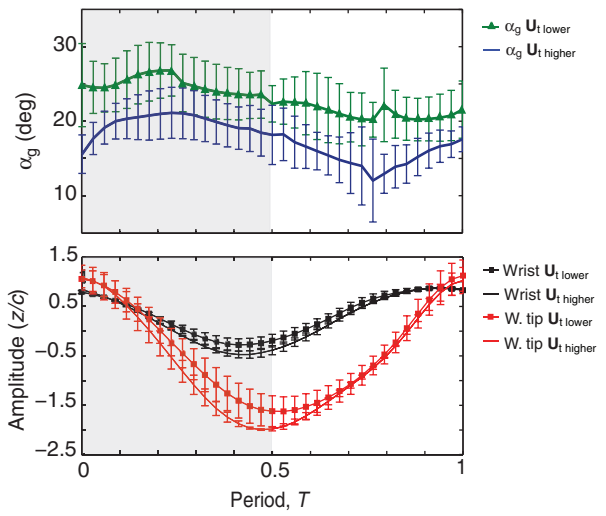

Fig. 3. Geometric angle of attack, vertical wrist and wingtip excursion at lower and higher wind speeds averaged over four bats (N=4, 5 wing cycles per bat and speed, except bat IV with only 3 at higher speed). Grey shading indicates downstroke.

because the kinematic parameters or average circulation did not differ significantly from trials with lower acceleration.

The geometric angle of attack, calculated at the wrist position, changed significantly between the lower and higher speed (Table 2; Fig. 3). For both speed categories, α_g increased at the beginning of the downstroke, reached its maximum value around mid-downstroke, and decreased thereafter, with a minimum approximately at mid-upstroke. The complex wing motion during the upstroke hindered the calculation of α_g for cases when the cross section between wing planform and wrist and trailing edge was located outside of the region between foot and fifth digit. Seven wing cycles in each speed category therefore showed gaps during part of the upstroke. The average of the remaining cycles, however, show positive values for α_g during the entire upstroke.

Wake structure and force generation

For all bats and at both speeds, we identified four distinct vortex structures in the wake whose appearance was correlated with particular phases of the wingbeat cycle (Figs 4, 5). The most dominant vortex structure was the tip vortex, V1, which started to develop at the beginning of the downstroke (Fig. 4A). The tip vortex grew in strength and diameter during the downstroke (Fig. 4, Fig. 5A,B), and persisted until almost the end of the upstroke. The position of the tip vortex in the wake was strongly correlated with the wingtip position; the tip vortex reached its maximum distal position when the wings were maximally extended, and was closer to the body during the upstroke, when the wings were retracted medially. The correlation between the wingtip and tip vortex positions was especially strong during the downstroke, with the vortex located slightly medial to the wingtip. This inward motion is in general agreement with the classical theoretical prediction for the motion of a tip vortex behind an aircraft wing in which the tip vortex lies at $z=\pi b/4$ (Betz, 1932). The strength and definition of the tip vortex started to decrease around mid-upstroke, and its close relationship with the wingtip position weakened (Fig. 5C). During this phase, the vorticity of V1 often was no longer confined within distinct vortex structures but rather was spread over a larger area that was swept by the curled wing during its upward motion (Fig. 5D). Around the lower reversal point and during the first half of the upstroke, V1 often developed a second vortex core (Fig. 5B,C,D), sometimes resulting in the development of two separate branches (Fig. 5E), with the inner branch in close proximity to the location of the tip of the fifth digit.

In addition to the onset of the tip vortex, a counter-rotating vortex, V2, appeared simultaneously, at the beginning of the downstroke, in close proximity to the body (Fig. 4A). This clockwise-rotating vortex generally persisted for approximately half of the downstroke, but in rare cases remained until after the lower reversal point at the end of the downstroke, although its duration varied considerably between different trials (e.g. Fig. 4, Fig. 5E isosurface reconstructions). During the last third of the upstroke, a pair of smaller vortices were also consistently observed: a proximal clockwise-rotating vortex, V3 (Fig. 4C, Fig. 5D, red), and a distal counterclockwise-rotating vortex, V4 (Fig. 4C, Fig. 5D, blue). These two vortices were always in close proximity to each other, generally located slightly medial to and above the wingtip. Aerodynamically similar to V1 and V2, these two vortices are part of a closed vortex loop, but rotate in the opposite direction to the lift-generating V1 and V2 system, generating negative lift at the distal part of the wing. V3, the medially located positive vortex that rotated in the same direction as the tip vortex, was often connected to the remaining diffuse vorticity of the tip vortex, whose location at this part of the wingbeat cycle was no longer exclusively linked to the wingtip, but had shifted medially or inboard, towards the fifth digit. The vortex pair, V3 and V4, generally persisted until the beginning of the downstroke, but was quickly displaced by the development of the tip vortex. This transition is easily spotted by the change in rotational direction of the distal or outward-located vortex, V4 (from negative vorticity to positive vorticity) as the tip vortex, V1, develops. Lower and higher speeds show a similar pattern of vortex development, characterized by the dominant tip vortex, V1, and its counter-rotating proximal vortex, V2, along with the secondary vortex pair, V3 and V4, in proximity to the upper reversal point.

The strength of the tip vortex, V1, increased relatively quickly with the onset of the downstroke, but leveled out shortly after, staying at a nearly constant value over the majority of its lifetime before it decreased to almost zero (Fig. 6). The development of the near-body counter-rotating vortex, V2, started simultaneously with the onset of the tip vortex. V2 then increased in strength until the tip vortex strength slowed in its rapid ascent, and then diminished. At the beginning of the development of V1 and V2, the difference in strength between the two vortices is well within the standard deviation. However, shortly afterwards, the slope of V2 generally decreases and it approaches its maximum at a slower rate. The two counter-rotating vortices that appeared at the end of the upstroke, V3 and V4, were considerably weaker than the primary tip vortex, and their presence alternated with the appearance of the tip vortex, although there was clear overlap when both structures were visible.

The average circulation over the entire wingbeat cycle decreased significantly with higher speed, whether evaluated over the entire wake area, ΓA_t (d.f.=30.2, t=5.36, P<0.001) or over the tip vortex V1 only (d.f.=35.2, t=3.73, P=0.001). By contrast, circulation of the three smaller vortices, V2 (d.f.=28.9, t=–0.67, P=0.509), V3 (d.f.=45.4, t=1.50, P=0.147) and V4 (d.f.=42.2, t=–1.43, P=0.159) did not change between lower and higher speeds (Fig. 7A). The duration of the tip vortex, VI, was significantly shorter at the higher speed (d.f.=35.4, t=3.47, P<0.001; Fig. 7B). However, the duration of the other vortex structures, V2 (d.f.=32.6, t=0.08, P=0.938), V3 (d.f.=34.0, t=0.66, P=0.534), and V4 (d.f.=33.9, t=0.42, P=0.703), did not change (Fig. 7B).

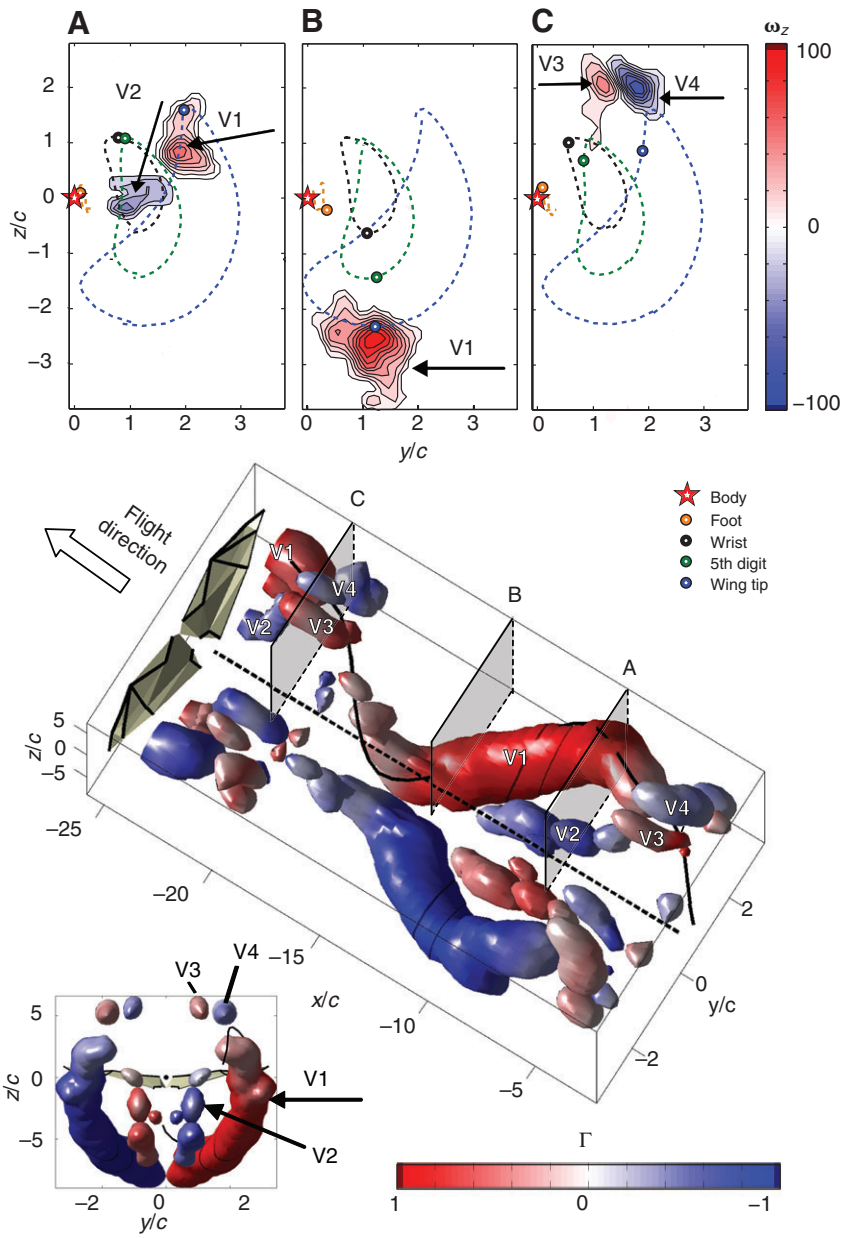

Fig. 4. Upper images: transverse vorticity fields at three positions over the wingbeat cycle at 7 m s^{-1}: upper reversal point (A), lower reversal point (B), end of upstroke (C). A vorticity threshold of 10 s^{-1} was applied and only consecutive vorticity patches of primary vortices are shown, eliminating any residual noise or smaller vortices (see text for vortex labels, colored bar: strength of vorticity). The images include the instantaneous position of body, foot, wrist, tip of the fifth digit and wingtip as well as the path over the wingbeat cycle. Distances are normalized by the average wing chord, *c*. See supplementary material Fig. S1 for vector fields. Lower image: reconstruction of the wake structure for approximately one and a half wingbeat cycles. Isosurfaces of the transverse swirl are shown based on the 2-D PIV images. The wake is displayed in the body reference coordinate system in the *y*–*z*-plane, and time was converted into space in order to allow the spatial display of the wake structure behind the bat. The wake structure was mirrored along the body trajectory line and colored based on the circulation of the four dominant vortex structures (V1–V4; blue: clockwise rotation, red: counter-clockwise rotation). Body (dashed line) and wingtip trajectory (solid line) are displayed for the right wing. The locations corresponding to the vorticity planes displayed above are indicated accordingly (A–C).

The mean circulation of V1 and mean angle of attack calculated over a wingbeat cycle are significantly correlated (d.f.=3.57, t=4.32, P=0.016). However, the temporal development of the circulation of V1 over the course of the cycle is not significantly linked to the instantaneous angle of attack (lower speed: d.f.=34.0, t=0.42, P=0.675; higher speed: d.f.=34.0, t=1.00, P=0.323). The instantaneous circulation values for V1 circulation, however, show a significant positive correlation with the instantaneous tip velocities (lower speed: d.f.=34.0, t=2.10, P=0.043; higher speed d.f.=34.0, t=3.71, P=0.0008), and tip velocity and angle of attack are correlated for higher speed (lower speed: d.f.=34.0, t=0.42, P=0.67, higher speed: d.f.=34.0, t=7.01, P<0.001). Neither the mean nor the instantaneous circulations of V2, V3 and V4 show a significant correlation with the mean instantaneous angle of attacks or velocities of the wing tip.

Differences between and within individual bats

We observed that the vortex generation over the wingbeat cycle follows a general pattern that was typical for all individual bats and both speeds. However, the large standard deviations seen in Figs 3, 6 and 7 indicate considerable variation between different wingbeat cycles in both the magnitude and duration of the circulation of the four vortices, as well as in kinematic parameters such as angle of attack, etc.

The path of bat wingtip can vary considerably, but is much more consistent in wingbeats and trials of a single individual (Fig. 8). There is a clear difference in wingtip trajectory between speeds for all bats, consistent with the significant change in tip-body distance, stroke plane angle and amplitude. However, in two of the four bats, the difference was especially distinctive (bat I and bat III in Fig. 8A,B,E,F). The standard deviations of wingbeat cycles were averaged for the *x*-, *y*- and *z*-directions for each individual bat and for all bats together. The greater consistency within individuals was reflected in the smaller standard deviations for the individuals compared with the larger standard deviation when averaged over all bats (Fig. 9A).

There was no significant difference between the two speeds in the mean standard deviation (averaged over the wing beat cycle) of

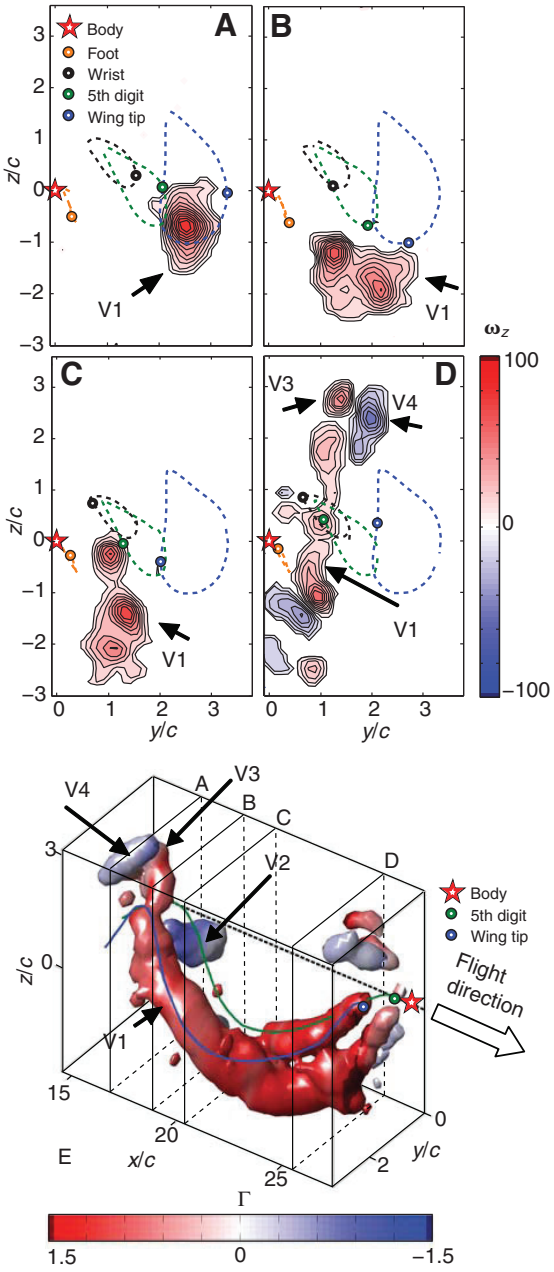

Fig. 5. Upper image: transverse 2-D vorticity fields at four positions over the wingbeat cycle at 5 m s^{-1}: mid-downstroke (A), lower reversal point (B), beginning of upstroke (C), mid-upstroke (D); for further descriptions see Fig. 4. See supplementary material Fig. S2 for vector fields. Lower image: reconstruction of the wake structure for the right wing. Isosurfaces of the transverse swirl are shown and the wake is displayed in the body reference coordinate system in the *y*–*z*-plane, and time was converted into space. The wake structure was colored based on the circulation of the four dominant vortex structures (V1–V4; blue: clockwise rotation; red: counter-clockwise rotation). Body (dashed line), wingtip (solid blue line) and fifth digit (solid green line) trajectory are displayed.

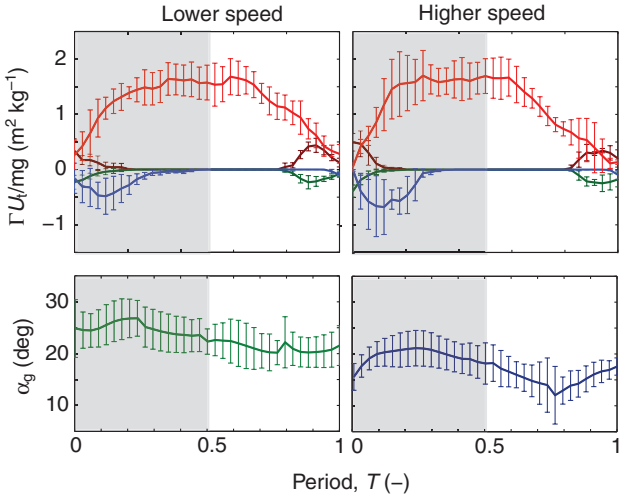

Fig. 6. Upper panels: development of the circulation divided by the body weight for all four vortices during the wingbeat cycle at lower and higher wind speeds averaged over four bats (*N*=4, 5 wing cycles per bat and speed, except bat IV with only 3 at higher speed). Lower panels: geometric angle of attack (removed at cycle) at lower and higher wind speeds. Grey shading indicates downstroke.

the wrist or wing tip trajectory within wingbeat cycles of the same bat (wrist: d.f.=3, t=–1.40, P=0.250; wing tip: d.f.=3, t=–0.45, P=0.682, N=60). By contrast, the mean standard deviation for all bats was not only higher in general, but markedly higher at lower speed (σ_{low}=0.0176, σ_{high}=0.0145), indicating that the differences between bats were more pronounced at the lower flight speed (Fig. 9A,B). Compared with the wingtip trajectory, differences in the path of the wrist were less pronounced, but consistent with the results of the wingtip analysis.

In order to examine whether individual bats differ significantly from this overall pattern, we repeated the kinematic analysis for individual bats using all available wingbeat cycles with wingbeat cycle as a repeated measure (Table 3). The change in kinematic parameters with speed differed between bats; every bat differed from the others in at least one kinematic trait. Three of the individuals showed significant differences in circulation between the two speed categories, and three out of four bats also showed a significant difference in the minimum body marker to wingtip distance. Wingbeat amplitude, stroke plane angle, and angle of attack differed for two bats, and downstroke ratio, maximum span and flapping frequency changed significantly for only one of the bats. Only three variables showed no significant changes with speed for any bat: horizontal and vertical acceleration, and wing chord.

Not only can the wing path vary substantially between individual bats and with changing speed, but also the development of the circulation can also differ considerably. The duration and strength of the near-body vortex, V2, differs most noticeably, being absent in some cases and stretching until almost the end of the downstroke under rare circumstances. The rise and fall of the circulation of the tip vortex differs both between individuals and also between different speeds of the same individual, with differences in slope and duration of constant circulation (Fig. 10).

DISCUSSION

Wake structure

The wake structure of *Cynopterus brachyotis* is similar at lower and higher flight speeds. The appearance of four different vortices in the *y*–*z*-plane over the course of one wingbeat cycle was the prevailing pattern observed for all four bats at both speeds. The dominant vortex structure is the tip vortex, V1, which is present over the majority of the wingbeat cycle, generating lift during the

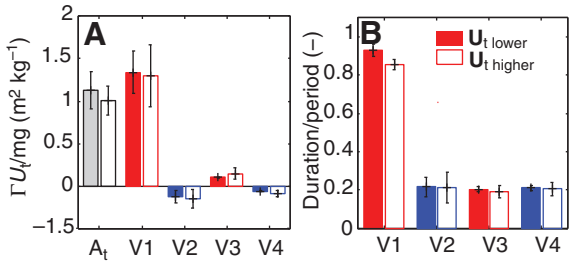

Fig. 7. (A) Average circulation generated over one wingbeat cycle based on the overall area (A_t) and for all four vortices at two speeds (N=20 at low speed, N=18 at higher speed). (B) Duration of appearance in relation to period time, which was determined between two local minima in the overall circulation.

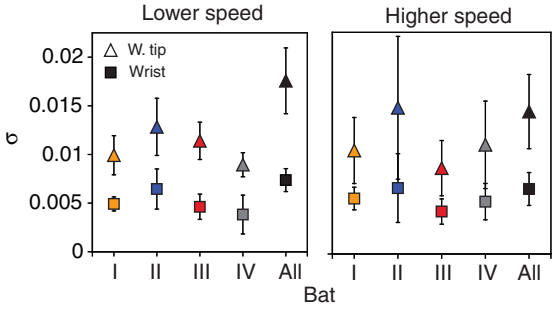

Fig. 9. The mean standard deviation, σ, from the path of the wing tip over one wingbeat cycle averaged over five wingbeat cycles from different trials for individual bats (except bat IV with only 3 at higher speeds), and 20 (18 at higher speed) wingbeat cycles for all bats together. The displayed standard deviation is an average of all three directions.

downstroke as well as over large parts of the upstroke. In spite of its long-term presence, the tip vortex diminishes considerably later in the upstroke, and disappears totally at the end of the upstroke, suggesting that the overall wake pattern is one of successive ring vortices rather than a continuous vortex structure, although gaps between the rings are small. The position of the tip vortex is strongly correlated with the wingtip position during the downstroke, although positioned slightly inwards and below the tip location. Simultaneous to the formation of the tip vortex, a counter-rotating vortex, V2, develops at the beginning of the downstroke. V2 increases in strength simultaneously with V1, but disappears gradually towards mid-downstroke. V2 is located in close proximity to the body, and shows vertical displacement similar to V1 over the course of its existence, most probably because of the strong downward momentum of the flow behind the bat. However, unlike V1, for which the vertical and horizontal location is closely related to the wing tip position, V2 shows very little horizontal displacement, suggesting its origin more closely related to body position rather that the fifth digit trajectory.

During the first half of the upstroke, V1 shifts medially and loses strength as well as its distinct contour. At the end of the upstroke, a second vortex pair, V3 and V4, appears in the distal wing region, with the more proximal vortex of the pair, V3, rotating in the same direction as the inward-shifted tip vortex, V1. The appearance of vortex pair V3 and V4 is similar to the pair identified in the wake of *Glossophaga soricina* (Hedenström et al., 2007). The vertical

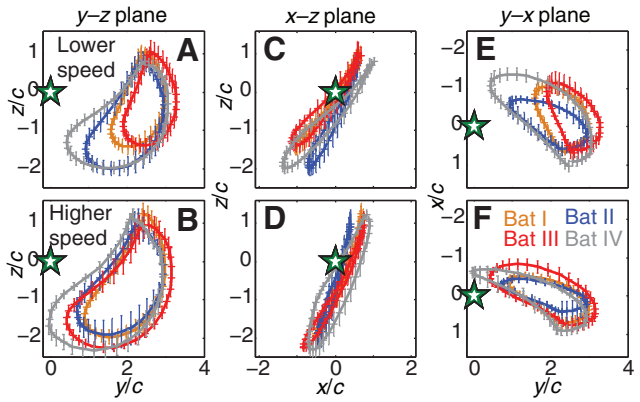

Fig. 8. Average wingtip trajectory in body reference coordinate system, normalized by the wing chord, for four bats in the *y*–*z*-plane, x–*y*-plane and *y*–*x*-plane (note reverse ordinate *y*–*x*-plane). Body marker position indicated by a star.

distance between the two vortices V1 and V3 in the far field is a result of the upwash of the distal vortex pair V3 and V4 and the downwash of the medially shifted vortex, V1, leading to a vertical displacement of both V1 and V3, although both probably originate in close proximity to the tip of the fifth digit (Johansson et al., 2008).

The existence of the two small vortices, V3 and V4, is consistent with kinematics-based predictions of negative vertical forces at the distal wing region (Norberg, 1976b) as well as wake measurements from *Glossophaga soricina* at medium (4 m s^{-1}) and high speed (6.5 m s^{-1}) (Hedenström et al., 2007; Johansson et al., 2008). The simultaneous existence of a tip vortex, V1, and the distal vortex pair, V3 and V4, indicates that the distal portion of the wing generates negative lift while the proximal wing is generating positive lift. However, although Norberg presumed negative vertical net forces for *Plecotus auritus* during most of the upstroke from determination of negative angles of attack, the strength and duration of the distal vortices V3 and V4 in our measurements from *Cynopterus brachyotis* suggest that positive lift generation prevails during the majority of the upstroke, with negative lift generated only near the upper reversal point. This view of positive lift generation at the proximal part of the wing is supported by evidence from the geometric angles of attack at the wrist (Fig. 3), showing positive geometric angles of attack over the entire wingbeat cycle, consistent with positive lift generation over large parts of the wing, even during the upstroke.

Although there are similarities between the wake structures we find here for *C. brachyotis* and those found at medium and high speed for *Glossophaga soricina*, such as the distal vortex pair at the end of the upstroke, there are also distinct differences between the wakes reported for this very small hovering specialist and the substantially larger bat studied here. In the present study, the onset of the tip vortex development is accompanied by a counter-rotating proximal vortex, V2. However, unlike the situation for *Glossophaga*, in which this vortex is continually generated close to the body, it persists for considerably less time in *C. brachyotis*. This indicates that the wings of *C. brachyotis* act as two distinct, separate wings at the beginning of the downstroke, but quickly start acting as a single system, including the body, with respect to lift generation. This is illustrated in Fig. 11A, which shows a sketch of the distribution of the circulation based on the appearance of the vortices in the transverse plane. At the beginning of the downstroke, each wing acts separately, as indicated by the synchronous development of the tip (V1) and near-body (V2) vortex. As the near-body vortex disappears, the separate right and left wings start to work as a single system, significantly increasing the circulation in the near-body

Table 3. Comparison of kinematic parameters between lower and higher speed flights for each bat

	Bat I n_1=5 n_2=19	Bat II n_1=5 n_2=5	Bat III n_1=5 n_2=10	Bat IV n_1=8 n_2=3
Frequency, f (Hz)	0.191	0.965	0.040	0.263
Amplitude, θ_{tip} (deg)	<0.001	0.393	0.001	0.062
Downstroke ratio, τ (–)	0.416	0.348	0.001	0.318
Horizontal acceleration, $\mathbf{a}_x$ (m s^{-2})	0.159	0.999	0.202	0.906
Vertical acceleration, $\mathbf{a}_z$ (m s^{-2})	0.816	0.999	0.633	0.199
Stroke plane angle, β (deg)	<0.001	0.557	0.620	0.005
Max. span (one wing), b (m)	0.383	0.324	0.186	0.040
Max. wing chord, c (m)	0.882	0.254	0.229	0.160
Min. distance body – wing tip, d_{min} (m)	0.041	0.222	0.003	0.001
Span ratio SR (–)	0.541	0.135	0.061	0.427
Geometric angle of attack, α_g (deg)	0.001	0.530	0.274	0.014
Circulation A_t, Γ (m s^{-2})	<0.001	0.035	0.170	<0.001

P-values for lower *versus* higher speed; *n* is the number of wingbeat cycles used for calculation; lower speed is n_1; higher speed is n_2. Shaded values are significant.

region (Fig. 11A). Owing to the wings' flapping motion, the distribution of the circulation over the span changes considerably over the wingbeat cycle. Measurements behind a mechanical flapping model showed a decrease in circulation in the near-body region to zero or almost zero at the reversal points, indicating that no lift is generated by the body itself (Hubel and Tropea, 2009). However, with the beginning of both the downstroke and the upstroke, the circulation over the body increases considerably although the body position does not change. Further investigation of the influence of dihedral angle and flapping motion on force

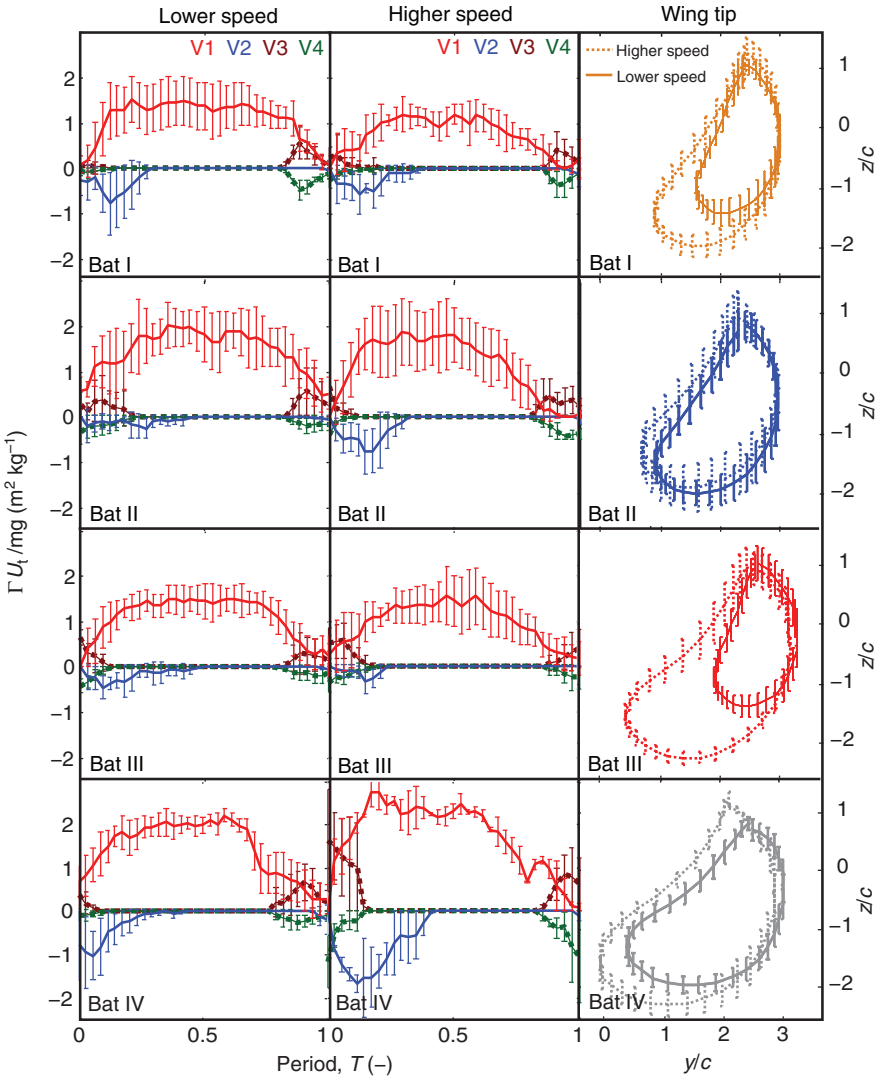

Fig. 10. Development of the circulation over the wingbeat cycle for all individuals and speeds including the wing tip trajectory at two speeds (solid line: lower speed; dashed line: higher speed, 5 wing cycles per bat and speed, except bat IV with only 3 at higher speed).

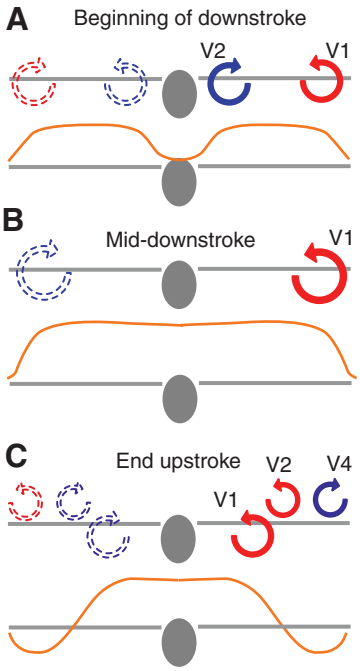

Fig. 11. Idealized schematic of the possible distribution of the circulation over the span for *Cynopterus brachyotis* at the beginning of downstroke, mid-downstroke and end of upstroke, based on the existence of tip, V1, body-near vortex, V2, and distal vortex pair V3 and V4. Grey: body and wings of bat from behind, orange line: possible distribution of the circulation.

generation in the near-body region could confirm or reject hypotheses concerning possible mechanisms for the increase in circulation in this region.

Based on the development of the geometric angle of attack, with its maximum around mid-downstroke, one might expect that the maximum circulation along the span shifts to the distal region at mid-downstroke (Hubel and Tropea, 2009). The shape of the circulation distribution would therefore continue to support the generation of a counter-rotating near-body vortex through the majority of the downstroke. However, the near-body vortex reaches its maximum strength before the maximum geometric angle of attack is reached, at approximately 25% of the downstroke (Fig. 6), and has almost disappeared by mid-downstroke. The disappearance of the near-body vortex during the downstroke suggests that during this phase, the entire body is acting as a single wing, and that the body has become an integral part of the lift generation (Fig. 11B), although measurements in the longitudinal plane, parallel to the flow, would be needed to properly confirm this hypothesis. Towards the end of the upstroke, the simultaneous appearance of the distal vortex pair, V3 and V4, along with the persistence of the tip vortex, suggests generation of negative circulation at the distal part of the wing (Fig. 11C).

Using the calculated angle of attack as explanation for the development of the circulation over the wingbeat cycle requires considerable caution. The continuously positive angles of attack over the entire wingbeat cycle suggest constant lift generation; however, the circulation clearly decreases to near zero in proximity to the upper reversal point (Fig. 6). Also, circulation remains fairly constant until the second third of the upstroke, but the angle of attack starts to decrease around mid-downstroke. Given the complexity of 3-D wing motions and resulting geometries of a highly compliant, stretching skin membrane, a geometric angle of attack calculated only at the wrist, with the trailing position located between tip of the fifth digit and foot, it is likely to be valid only for a very localized region of the wing, and not representative of larger areas of the wing either proximal or distal to the wrist. More detailed kinematic measurements and a more sophisticated marker set are necessary in order to gain insight into the development of the angle of attack along the span and over the wingbeat cycle, and might enable and subsequent analyses of correlation with circulation development.

Although we have not made wake measurements parallel to the flow, we have reconstructed the 3-D wake structure based on the information gained from the transverse plane measurements, which indicates the existence of shed vorticity, either in the form of a shear layer, or as discrete starting and stopping vortices, from the changes in the strength of the vortices measured in the transverse plane. Taking the roughly constant circulation over large parts of the down- and upstroke into account, we conclude that the shedding of vorticity in the parallel plane was mainly limited to the beginning of the downstroke and end of the upstroke (Fig. 12).

Four obvious vortex structures were identified over the wingbeat cycle, but additional smaller structures could exist and might not be identified due to the background noise level. This is more likely during the upstroke, when there are a number of small vorticity patches visible, probably related to the complex wing motion and increased body–wing interaction. In addition, only circulation in the streamwise direction could be resolved, underestimating the true circulation of inclined, and therefore diagonally cut, vortices.

Circulation in the near and far field

The PIV observation plane was located between two and 20 wing chords from the flying bats, and a single trial often contained multiple wingbeat cycles, starting in the near field, and ending in the far field, because of the upstream movement of the bat. Comparison between these wingbeat cycles shows that the vortex structures dissipate slightly with increasing distance, as one would expect. In addition, one can observe an increasing displacement of vortices because of vortex interaction with the downstream movement of the wake (Johansson et al., 2008). However, we found no significant correlation between distance behind the bat and strength of any of the four main vortices identified or the overall circulation. The constant total circulation confirms previous observations, where no significant influence of dissipation and flow unsteadiness was found over a range of two to 40 wing chords (Hubel et al., 2009), and is consistent with results from recent studies of bat wakes (Johansson et al., 2008). The lack of significant changes in the strength of the separate vortices with increased distance from the animal also shows that the vortex roll-up process was completed by the closest location at which the PIV plane sampled the wake, in agreement with studies of tip vortex development, which showed that rollup is finished approximately 1–1.5 chord lengths behind the wing (Birch and Lee, 2003). Measurements on swept and rectangular wings at Re=180,000 have also shown no significant change in circulation between 1 and 3.5 chord length behind the wing (Gerontakos and Lee, 2006). However, although circulation was not affected by increasing distance, it is possible that with increasing distance from the bat the likelihood that we might not adequately detect small vortex structures increases.

Absolute forces

It is common for PIV studies in animal flight to relate wake circulation to lift force using the Kutta–Joukowski theorem (Anderson, 2001). However, determining absolute lift values for our measurements is

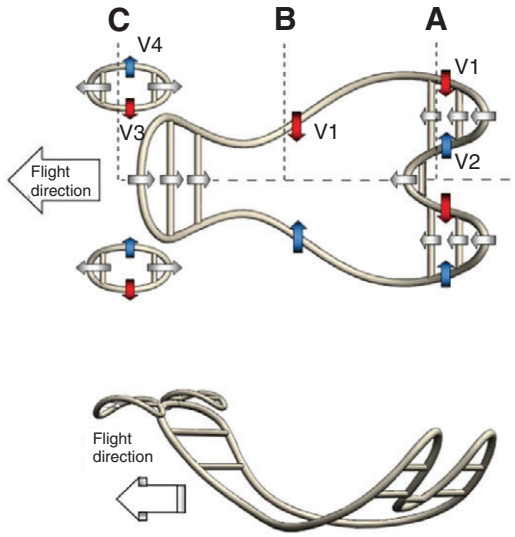

Fig. 12. Reconstruction of the 3-D wake structure based on the 2-D PIV measurements. Sections (A,B and C) correspond to the 2-D vorticity fields and 3-D isosurface reconstruction in Fig. 4. Red arrows: counter-clockwise rotating vortex; blue arrows: clockwise rotating vortex; grey arrows: predicted vorticity shed in the parallel plane (*x*–*z*-plane) either in the form of shear layers or starting and stopping vortices.

challenging for several reasons, including continuously changing wingspan and experimental challenges associated with time-resolved measurements in the transverse plane. The limits to generating adequate laser energy at high frequency, generating high densities of seeding particles, and maintaining adequate spatial resolution in a large PIV window all contribute to lower than expected values in the absolute magnitude of the circulation measured. This issue has been quantified in detail for a model system consisting of a fixed wing generating a comparable vortex structure as is reported here (Waldman et al., 2009). It was found that with our current available laser power of 50 mJ pulse^{-1} at 200 Hz, decreasing spatial resolution leads to a incompletely resolved streamwise vortex structure, and that although the vortex shape is correctly captured, the measured circulation is lower than the true circulation. In the series of experiments reported here, capturing the whole wingbeat cycle of the medium-sized bat required a large observation area with resolution of 0.24 mm pixel^{-1}, and we determined that the absolute magnitude of the circulation, and consequently the aerodynamic forces, to be underestimated by approximately 30%.

The circulation extracted from the transverse plane contains the vertical force component of lift whereas the magnitude of the horizontal forward force is not directly determined. Ultimately, the vertical force must balance body weight over the course of the wingbeat cycle if there is not significant vertical acceleration. We calculated the average vertical force generated over the course of a wingbeat cycle based on the tip vortex circulation, integrated over the instantaneous wing extension. The near-body vortex and distal vortex pair were neglected for this estimation, leading to an overestimate of force production. With these considerations in mind, we find that the vertical force calculated based on the circulation of the tip vortex gives a lift force value of 42.7% of the body weight, well below the 70% expected based on the low spatial resolution. The value was found to vary slightly depending on the PIV evaluation parameters.

To further explore the possible sources of the underestimation of lift in our measurements, we carried out a supplementary experiment. We readjusted the thickness and intensity distribution of the laser sheet and added a second seeding particle generator to test the hypothesis that these were the most important factors in our low lift magnitude estimates, and carried out four trials at lower and higher speed employing one bat (bat IV). In these trials, lift averaged 94.6% of body weight when based on tip vorticity. The overall structure of the wake and relative strengths of the distinct vortex structures were identical to those in all previous experiments reported here.

Kinematics and PIV correlation

The simultaneous recording of PIV and kinematics and the subsequent correlation between the two measurements allows us, in principle, to link vortex wake structures to specific geometric features of the wingbeat cycle, such as angle of attack. In addition, one can make associations between the instantaneous positions of marked locations on the wing and vorticity features in the wake. However, as mentioned earlier, this association is difficult, as one has to consider the effects of vortex interactions and resulting displacements generated by the induced velocities with increasing distance between the trailing edge and observation plane. During the downstroke, although the tip vortex is shifted slightly inward and located below the wing tip, the correlation with the position of the wing tip is apparent (Fig. 5A). At the beginning of the upstroke, there is an additional inward shift, and the tip vortex loses its close association with the wing tip position. At this stage of the cycle, the direct correlation between positions on the wing and the generated vortex structure becomes challenging. The wings are pulled towards the body and the two tip vortices are quite close to each other, and thus influence each other strongly. During this phase of the wingbeat cycle, the tip vortex often develops a secondary vortex core (Fig. 5B,C,D,E). Some of the trials show what seems to be a distinct split of the tip vortex into two branches, with the inner branch in close proximity to the location of the tip of the fifth digit. However, more often the pattern is much less distinct. Wing motion, the more vertical orientation of the distal wing, and the influence of the body and other secondary vortex structures all contribute to a more complex pattern of vortex advection from the body to the PIV measurement plane, making the association between vortex structures and specific features on the body difficult if not impossible during this phase of the wingbeat cycle. From these experiments alone, it is not possible to determine conclusively whether the secondary vortex core structure is a result of a change in the distribution of the circulation over the wing or is founded in vortex–vortex or vortex–body interactions.

Individual differences

There are considerable differences in the wing path trajectory between individuals and the two speeds, as well as in the adjustment of flight parameters between speeds. Amplitude, stroke plane angle, and body-to-wingtip distance (‘curling’) are the most consistent parameters to vary between the two speed categories, suggesting that their influence on aerodynamic forces can be important. The differences in body-to-wingtip distance between the speeds is especially obvious for bat I and bat III, which maintain a considerably larger body-to-wingtip distance at the lower speed than the other two bats. At higher speed, the difference is less pronounced, and all the bats pull their wings closer to the body on the upstroke. Downstroke ratio, maximum span and frequency changed less often between the two speed categories; one might speculate that their purpose might be that of fine tuning rather than the change in speed

itself. The results regarding the significance of frequency and downstroke ratio in *Cynopterus* stand in contrast to other species that show a significant change in frequency (Norberg and Winter, 2006; Wolf et al., 2010) and downstroke ratio (Wolf et al., 2010) with speed, but are in agreement with measurements used for comparing kinematics of differently sized pteropodid bats (Riskin et al., 2010). Out of six species investigated three did not show a significant change in frequency with speed and only two showed significant change in downstroke ratio. Surprisingly, for bat II, there were no significant differences between speeds in any of the parameters we described. However, the relative lack of kinematic differences between lower and higher speed overall and in this bat in particular suggests that parameters yet to be considered are likely to be relevant to regulating flight speed. These results also provide additional evidence that individual bats vary in the ways in which diverse flight parameters may be modulated to change the flight speed (Iriarte-Diaz, 2008). The high degree of individual variation shows that the sample size can greatly influence the significance of certain flight parameters. General statements regarding the importance of certain parameters for a species based on the investigation of only four or five individuals must be regarded with some caution (Iriarte-Diaz and Swartz, 2008; Riskin et al., 2010) and are more tentative for even smaller sample sizes (Norberg and Winter, 2006; Wolf et al., 2010).

Linking individual differences in kinematic strategies to specific individual variations in morphology, such as body mass, wing loading or bone architecture, is a challenging but potentially rewarding avenue for future research.

The development of circulation of the tip vortex also differs between individuals and between speeds. Higher speed seems to be associated with a shorter duration of constant circulation and an earlier onset of the decrease in circulation. The two bats that exhibit less curling in their wings during the upstroke at lower speed, bats I and III, also show steep changes in circulation at the beginning and end of the wingbeat cycle and a long phase of nearly constant circulation in between. These two observations may or may not be related, and the causality between the development of circulation and wing path trajectory, angle of attack, and other kinematic parameters would benefit from further investigation. The standard deviation of the circulation is considerably higher than of the two-dimensional wing path trajectory, considering the differences in all three dimensions and other flight parameters, suggesting that we have yet to identify the complete kinematic basis of the production of the measured circulation.

Conclusions

We consistently identified four vortex structures as typical for both lower and higher speed flight in *Cynopterus brachyotis*. The wake structure was dominated by a strong tip vortex that developed during the downstroke and remained until almost the end of the upstroke. However, although the portion of the wingbeat cycle with no tip vortex was very short, the wake structure can still be considered a vortex ring rather than a continuous vortex structure. The proportion of the cycle without the presence of the tip vortex increased with speed; this contrasts with the continuous vortex or ladder structure at higher speeds that has been proposed for bird flight based on both observations and theory (Rayner and Gordon, 1998; Hedrick et al., 2002; Tobalske et al., 2007; Henningsson et al., 2008). Simultaneously with the onset of the tip vortex at the beginning of the downstroke, a counter-rotating near-body vortex developed, indicating that the left and right wings operate independently, with no or little lift generation over the body. However, shortly afterwards the near-body vortex diminished, leaving the two wings, including the body, operating as a single airfoil. A pair of two small vortices appears at the end of the upstroke at the distal part of the wing, a sign of negative lift, accompanied by thrust generation at the distal part of the wing. However, drag and positive lift at the proximal wing prevail during most of the duration of the distal vortex pair due to the concurrent persistence of the tip vortex. Wing kinematics, as well as the development and strength of both the tip and near-body vortices, vary between individuals and speeds. However, finding direct causality between the development of the circulation and kinematics is challenging because of the number of changing parameters, and is an exciting challenge for future research.

ACKNOWLEDGEMENTS

We thank Nickolay Hristov, Arnold Song and Rye Waldman for helpful discussions, and Anthony Assad, Zachary Levko, Leigh MacAyeal, Alex Robb and Allyce Sullivan for handling and training of animals and their help with data collection. Andrew Bearnot helped design and create Fig. 12. We thank the Lubee Bat Conservancy, especially Allyson Walsh, for long term access to the bats. This work was supported by the Air Force Office of Scientific Research, monitored by Rhett Jeffries, Willard Larkin and John Schmisseur, and the National Science Foundation.

LIST OF ABBREVIATIONS

A	area
$\mathbf{a}_x$	horizontal acceleration
$\mathbf{a}_z$	vertical acceleration
b	span of one wing
c	wing chord
$d_{\min}$	minimum distance between body and wing tip
dt	time between images
dt_{new}	time used to correct for Doppler shift
f	wingbeat frequency
h	height
k	reduced frequency
Re	Reynolds number
SR	span ratio
T	wingbeat period
$\mathbf{U}_\infty$	free-stream (wind tunnel) velocity
$\mathbf{U}_B$	speed of bat, relative to test section
$\mathbf{U}_t$	total air speed of bat, $\mathbf{U}_\infty$–$\mathbf{U}_B$
V1	tip vortex
V2	near body vortex
V3	positive distal vortex
V4	negative distal vortex
α_g	geometric angle of attack
β	stroke plane angle
β_G	dimensionless height (β_G=*h*/*b*)
Γ	circulation
ΓA_t	circulation based on total area right of body position
θ_{tip}	amplitude of wing tip
ν	kinematic viscosity
ρ	air density
σ	standard deviation
τ	downstroke ratio
$\boldsymbol{\omega}$	vorticity

REFERENCES

Abdel-Aziz, Y. I. and Karara, H. M. (1971). Direct linear transformation from comparator coordinates into object space coordinates in close-range photogrammetry. In *Proceedings of the Symposium on Close-Range Photogrammetry*, pp. 1-18. Falls Church, VA: American Society of Photogrammetry.

Adrian, R. J., Christensen, K. T. and Liu, Z. C. (2000). Analysis and interpretation of instantaneous turbulent velocity fields. *Exp. Fluids* **29**, 275-290.

Aldridge, H. D. (1986). Kinematics and aerodynamics of the greater horseshoe bat, *Rhinolophus ferrumequinum*, in horizontal flight at various flight speeds. *J. Exp. Biol.* **126**, 479-497.

Anderson, J. D. (2001). *Fundamentals of Aerodynamics*. McGraw Hill.

Betz, A. (1932). Verhalten von Wirbelsystemen. *Zeitschrift fur angewandte Mathematikund Mechanik* **12**, 164-174.

Birch, D. and Lee, T. (2003). The roll-up and near field behavior of a tip vortex. *J. Aircr.* **40**, 603-607.

Birch, J. M. and Dickinson, M. H. (2001). Spanwise flow and the attachment of the leading-edge vortex on insect wings. *Nature* **412**, 729-733.

Birch, J. M. and Dickinson, M. H. (2003). The influence of wing-wake interactions on the production of aerodynamic forces in flapping flight. *J. Exp. Biol.* **206**, 2257-2272.
Bomphrey, R. J., Lawson, N. J., Harding, N. J., Taylor, G. K. and Thomas, A. L. R. (2005). The aerodynamics of *Manduca sexta*: digital particle image velocimetry analysis of the leading-edge vortex. *J. Exp. Biol.* **208**, 1079-1094.
Dickinson, M. H. and Gotz, K. G. (1996). The wake dynamics and flight forces of the fruit fly *Drosophila melanogaster*. *J. Exp. Biol.* **199**, 2085-2104.
Dickinson, M. H., Lehmann, F. and Sane, S. P. (1999). Wing rotation and the aerodynamic basis of insect flight. *Science* **284**, 1954-1960.
Ellington, C. P. (1999). The novel aerodynamics of insect flight: applications to micro-air vehicles. *J. Exp. Biol.* **202**, 3439-3448.
Gerontakos, P. and Lee, T. (2006). Near-field tip vortex behind a swept wing model. *Exp. Fluids* **40**, 141-155.
Hartley, R. and Zissermann, A. (2000). *Multiple View Geometry in Computer Vision.* Cambridge: Cambridge University Press.
Hedenström, A., Rosén, M. and Spedding, G. R. (2006). Vortex wakes generated by robins Erithacus rubecula during free flight in a wind tunnel. *J. R. Soc. Interface* **3**, 263-276.
Hedenström, A., Johansson, L. C., Wolf, M., von Busse, R., Winter, Y. and Spedding, G. R. (2007). Bat flight generates complex aerodynamic tracks. *Science* **316**, 894-897.
Hedenström, A., Muijres, F., von Busse, R., Johansson, L., Winter, Y. and Spedding, G. (2009). High-speed stereo DPIV measurement of wakes of two bat species flying freely in a wind tunnel. *Exp. Fluids* **46**, 923-932.
Hedrick, T. L., Tobalske, B. W. and Biewener, A. A. (2002). Estimates of circulation and gait change based on a three-dimensional kinematic analysis of flight in cockatiels (*Nymphicus hollandicus*) and ringed turtle-doves (*Streptopelia risoria*). *J. Exp. Biol.* **205**, 1389-1409.
Henningsson, P., Spedding, G. R. and Hedenström, A. (2008). Vortex wake and flight kinematics of a swift in cruising flight in a wind tunnel. *J. Exp. Biol.* **211**, 717-730.
Hubel, T. and Tropea, C. (2009). Experimental investigation of a flapping wing model. *Exp. Fluids* **46**, 945-961.
Hubel, T., Hristov, N., Swartz, S. M. and Breuer, K. S. (2009). Time-resolved wake structure and kinematics of bat flight. *Exp. Fluids* **46**, 933-943.
Iriarte-Diaz, J. (2008). Flight performance in bats and its ecomorphological implications. PhD thesis, Department of Ecology and Evolutionary Biology, Brown University, Providence.
Iriarte-Diaz, J. and Swartz, S. M. (2008). Kinematics of slow turn maneuvering in the fruit bat *Cynopterus brachyotis*. *J. Exp. Biol.* **211**, 3478-3489.
Johansson, L. C. and Hedenström, A. (2009). The vortex wake of blackcaps (*Sylvia atricapilla* L.) measured using high-speed digital particle image velocimetry (DPIV). *J. Exp. Biol.* **212**, 3365-3376.
Johansson, L. C., Wolf, M., von Busse, R., Winter, Y., Spedding, G. R. and Hedenström, A. (2008). The near and far wake of Pallas' long tongued bat (*Glossophaga soricina*). *J. Exp. Biol.* **211**, 2909-2918.
Lindhe Norberg, U. M. and Winter, Y. (2006). Wing beat kinematics of a nectar-feeding bat, *Glossophaga soricina*, flying at different flight speeds and Strouhal numbers. *J. Exp. Biol.* **209**, 3887-3897.
Lu, Y., Shen, G. X. and Lai, G. J. (2006). Dual leading-edge vortices on flapping wings. *J. Exp. Biol.* **209**, 5005-5016.
Muijres, F. T., Johansson, L. C., Barfield, R., Wolf, M., Spedding, G. R. and Hedenström, A. (2008). Leading-edge vortex improves lift in slow-flying bats. *Science* **319**, 1250-1253.
Norberg, U. M. (1976a). Aerodynamics of hovering flight in the long-eared bat *Plecotus auritus*. *J. Exp. Biol.* **65**, 459-470.
Norberg, U. M. (1976b). Aerodynamics, kinematics, and energetics of horizontal flapping flight in the long-eared bat *Plecotus auritus*. *J. Exp. Biol.* **65**, 179-212.
Norberg, U. M. L. and Winter, Y. (2006). Wing beat kinematics of a nectar-feeding bat, Glossophaga soricina, flying at different flight speeds and Strouhal numbers. *J. Exp. Biol.* **209**, 3887-3897.
Rayner, J. M. V. (1991). On the aerodynamics of animal flight in ground effect. *Philos. Trans. R Soc. Lond., B, Biol. Sci.* **334**, 119-128.
Rayner, J. M. V. and Gordon, R. (1998). Visualization and modelling of the wakes of flying birds. In *Biona Report 13, Motion Systems* (ed. R. Blickhan, A. Wisser and W. Nachtigall), Jena: Gustav Fischer Verlag.
Riskin, D. K., Willis, D. J., Iriarte-Díaz, J., Hedrick, T. L., Kostandov, M., Chen, J., Laidlaw, D. H., Breuer, K. S. and Swartz, S. M. (2008). Quantifying the complexity of bat wing kinematics. *J. Theor. Biol.* **254**, 604-615.
Riskin, D. K., Bahlman, J. W., Hubel, T. Y., Ratcliffe, J. M., Kunz, T. H. and Swartz, S. M. (2009). Bats go head-under-heels: the biomechanics of landing on a ceiling. *J. Exp. Biol.* **212**, 945-953.
Riskin, D. K., Iríarte-Diaz, J., Middleton, K. M., Swartz, S. M. and Breuer, K. S. (2010). The effect of body size on the wing movements of pteropodid bats, with insights into thrust and lift production. *J. Exp. Biol.* (in press).
Sane, S. P. (2003). The aerodynamics of insect flight. *J. Exp. Biol.* **206**, 4191-4208.
Spedding, G. R., Hedenström, A. and Rosén, M. (2003a). Quantitative studies of the wakes of freely flying birds in a low-turbulence wind tunnel. *Exp. Fluids* **34**, 291-303.
Spedding, G. R., Rosén, M. and Hedenström, A. (2003b). A family of vortex wakes generated by a thrush nightingale in free flight in a wind tunnel over its entire natural range of flight speeds. *J. Exp. Biol.* **206**, 2313-2344.
Spedding, G., Hedenström, A. and Johansson, L. (2009). A note on wind-tunnel turbulence measurements with DPIV. *Exp. Fluids* **46**, 527-537.
Tian, X., Iriarte-Diaz, J., Middleton, K., Galvao, R., Israeli, E., Roemer, A., Sullivan, A., Song, A., Swartz, S. and Breuer, K. (2006). Direct measurements of the kinematics and dynamics of bat flight. *Bioinspir. Biomim.* **1**, 10-18.
Tobalske, B. W., Hedrick, T. L., Dial, K. P. and Biewener, A. A. (2003). Comparative power curves in bird flight. *Nature* **421**, 363-366.
Tobalske, B. W., Warrick, D. R., Clark, C. J., Powers, D. R., Hedrick, T. L., Hyder, G. A. and Biewener, A. A. (2007). Three-dimensional kinematics of hummingbird flight. *J. Exp. Biol.* **210**, 2368-2382.
Usherwood, J. R. and Ellington, C. P. (2002). The aerodynamics of revolving wings I. Model hawkmoth wings. *J. Exp. Biol.* **205**, 1547-1564.
Usherwood, J. R., Hedrick, T. L. and Biewener, A. A. (2003). The aerodynamics of avian take-off from direct pressure measurements in Canada geese (*Branta canadensis*). *J. Exp. Biol.* **206**, 4051-4056.
van den Berg, C. and Ellington, C. P. (1997). The vortex wake of a "hovering" model hawkmoth. *Philos. Trans. R. Soc. B. Biol. Sci.* **352**, 317-328.
Waldman, R., Kudo, J. and Breuer, K. S. (2009). Trailing vortices from low speed flyers. APS/DFD meeting abstract. Minneapolis MN. http://meetings.aps.org/link/BAPS.2009.DFD.PT.2
Warrick, D. R., Tobalske, B. W. and Powers, D. R. (2005). Aerodynamics of the hovering hummingbird. *Nature* **435**, 1094-1097.
Wolf, M., Johansson, L. C., von Busse, R., Winter, Y. and Hedenstrom, A. (2010). Kinematics of flight and the relationship to the vortex wake of a Pallas' long tongued bat (*Glossophaga soricina*). *J. Exp. Biol.* **213**, 2142-2153.